Localized, Stepwise Template Growth of Functional Nanowires from an Amino Acid-Supported Framework in a Microfluidic Chip

Josep Puigmartí-Luis,[†,*] Marta Rubio-Martínez,[‡] Inhar Imaz,[‡] Benjamin Z. Cvetković,[§] Llibertat Abad,[⊥] Angel Pérez del Pino,[†] Daniel Maspoch,[‡,∥] and David B. Amabilino[†,*]

[†]Institut de Ciència de Materials de Barcelona (ICMAB-CSIC), Campus Universitari de Bellaterra, 08193 Bellaterra, Spain, [‡]ICN2—Institut Catala de Nanociencia i Nanotecnologia, Campus Universitari de Bellaterra, 08193 Bellaterra (Barcelona), Spain, [§]Laboratory for Waste Management, Department for Nuclear Energy and Safety Research, Paul Scherrer Institut, Villigen, Switzerland, [⊥]Institut de Microelectrònica de Barcelona, IMB-CNM (CSIC), Campus Universitari de Bellaterra, 08193 Bellaterra, Barcelona, Spain, and [∥]Institució Catalana de Recerca i Estudis Avançats (ICREA) 08100 Barcelona, Spain

ABSTRACT A spatially controlled synthesis of nanowire bundles of the functional crystalline coordination polymer (CP) Ag(I)TCNQ (tetracyanoquinodimethane) from previously fabricated and trapped monovalent silver CP (Ag(I)Cys (cysteine)) using a room-temperature microfluidic-assisted templated growth method is demonstrated. The incorporation of microengineered pneumatic clamps in a two-layer polydimethylsiloxane-based (PDMS) microfluidic platform was used. Apart from guiding the formation of the Ag(I)Cys coordination polymer, this microfluidic approach enables a local trapping of the *in situ* synthesized structures with a simple pneumatic clamp actuation. This method not only enables continuous and multiple chemical events to be conducted upon the trapped structures, but the excellent fluid handling ensures a precise chemical activation of the amino acid-supported framework in a position controlled by interface and clamp location that leads to a site-specific growth of Ag(I)TCNQ nanowire bundles. The synthesis is conducted stepwise starting with Ag(I)Cys CPs, going through silver metal, and back to a functional CP (Ag(I)TCNQ); that is, a novel microfluidic controlled ligand exchange (CP → NP → CP) is presented. Additionally, the pneumatic clamps can be employed further to integrate the conductive Ag(I)TCNQ nanowire bundles onto electrode arrays located on a surface, hence facilitating the construction of the final functional interfaced systems from solution specifically with no need for postassembly manipulation. This localized self-supported growth of functional matter from an amino acid-based CP shows how sequential localized chemistry in a fluid cell can be used to integrate molecular systems onto device platforms using a chip incorporating microengineered pneumatic tools. The control of clamp pressure and in parallel the variation of relative flow rates of source solutions permit deposition of materials at different locations on a chip that could be useful for device array preparation. The *in situ* reaction and washing procedures make this approach a powerful one for the fabrication of multicomponent complex nanomaterials using a soft bottom-up approach.

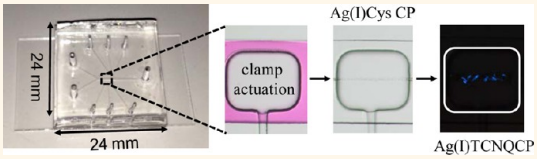

KEYWORDS: molecular nanomaterials · flow · template synthesis · amino acids · molecular electronics

The localization and integration of functional materials on surfaces is important for rapid device fabrication,[1] and bottom-up chemical approaches are particularly attractive. Among the several approaches employed so far, templated growth techniques have proven to be the most effective methods to localize and control the growth of monodisperse functional structures with nanoscale spatial resolution.[2,3] Nonetheless, in many cases, these approaches are time-consuming, labor intensive, and frequently require the use of expensive equipment. Therefore, a longstanding challenge in the field is to develop new approaches where sequential multiple chemical modifications can be performed under controlled mild conditions economically without the need for postassembly manipulation that could affect the performance of the material. Recently, for example, the templated growth approach to functional nanocrystals with the assistance of biomolecules has gained much attention owing to the ease with which extremely complex structures can be constructed from the bottom-up in a flexible manner with no need of expensive equipment and under mild conditions.[4,5] Biomolecular scaffolding of functional assemblies is an attractive and an emerging field of research in which a wide number of functional structures can be used for nanotechnological applications

* Address correspondence to jpuigmarti@icmab.es, amabilino@icmab.es.

Received for review October 21, 2013 and accepted December 19, 2013.

Published online December 19, 2013
10.1021/nn4054864

and device fabrication.[6−9] Within the various biomolecular scaffolding approaches, a set of coordination polymers (CPs) involving peptide-supported frameworks have proven to be relevant materials for a controlled template growth of functional superstructures at both, micro- and nanoscale dimensions.[10] Typically, CPs are crystalline materials that are composed of metal ion nodes coordinated to organic ligands.[11,12] While significant research efforts are focused in the development of novel synthetic methods for new CPs and while modification of the structure and composition of CPs is necessary in order to expand their number of functions to go beyond the state-of-the-art in certain applications, very little is known in terms of CPs acting as template scaffolds for the growth of functional materials that could be useful for introducing components in devices in a bottom-up way.

Common and straightforward methods employed so far to induce novel functions to CPs include establishing functional organic linkers in the structure[13,14] or inducing photochemical processes that can favor the reduction of the metal ions which act as nodes or connectors. For example, a direct-writing of microscopic metallic silver patterns inside single metal−organic crystals employing a laser beam approach has been reported recently.[15] Moreover, Cohen and co-workers have effectively reported postsynthetic organic linker modification approaches to porous CP crystals.[16−20] These studies have demonstrated effectively that tunable chemical and physical properties (*e.g.*, hydrophobicity or microporosity, respectively) can be modulated when CP crystals are subjected to postsynthetic modifications. Despite the progress achieved in this area, a major challenge that remains is to define rational and systematic methods that can enable the synthesis of novel functional structures grown from CP scaffolds and which could display distinct functionality to the former building blocks. For example, we have recently described the formation of Ag_2S semiconductor nanoparticles from a silver-cysteine (Ag(I)Cys) based CP after e-beam exposure.[21] Nonetheless, it should be emphasized that to impart functionality to CPs by treating and tuning their building block composition chemically is still largely unexplored.

Here we provide the first strong evidence that CPs can be used as scaffolds to template the growth of functional nanometer scale matter through sequential chemical reactions, and we further explore this templated growth mechanism with a two-layer microfluidic platform incorporating microengineered fluidic clamps, where a spatially resolved crystal template growth process is accomplished. In contrast to other templated growth routes where microscale porous CP crystals are modified by CP-on-CP heteroepitaxy,[22,23] or where CPs are grown on microscale nucleation agents,[24] we prove a silver-tetracyanoquinodimethane (Ag(I)TCNQ) templated crystal growth from a previously formed and immobilized amino acid-supported framework (Ag(I)Cys) which acts as the backbone scaffold in the process. Ag(I)TCNQ CPs are well-known charge transfer complexes with very interesting electroactive properties, for instance, for the fabrication of organic memory elements thanks to the existence of two reversible and stable electronic states. That is, the resistivity of this charge transfer complex switches from a high conductive state (ON state) to a low conductive state (OFF state) while changing the voltage applied to the complex.[24,25] In addition, the approach used to localize growth involves square-shaped microengineered fluidic clamps that can be actuated over electrode arrays located at the bottom of the fluidic layer which permitted the integration of Ag(I)TCNQ nanowire bundles to read-out components and at desired locations on a surface. To the best of our knowledge, there are no examples reported so far which combine sequential chemical event treatments, a functional crystal template growth method, where a microfluidic assisted ligand exchange is favored, and the actuation of microengineered pneumatic tools toward the assembly of fully integrated systems on surfaces. Thus, devices can be prepared on-chip from solution, with components at specific locations and that require no further manipulation that might affect the molecular material that is used.

RESULTS AND DISCUSSION

Double-layer microfluidic chips with square-shaped embedded deformable features were employed in our research. As shown in Figure 1a, the chips consisted of two layers of polydimethylsiloxane (PDMS) where the bottom-layer was designed to accommodate the fluidic channel and a top control layer was used to partially squeeze (using nitrogen gas) the fluidic channel toward the glass substrate (see Materials and Methods section for further details). This partial deformation of the fluidic layer resulted in what are effectively microengineered fluidic clamps (Figure 1). Determining the performance of these clamps and the behavior of the laminar flow upon clamp pressurization with nitrogen gas was necessary prior to Ag(I)Cys CP trapping. We studied the efficiency of the device with the injection of an aqueous solution of rhodamine dye through the fluidic layer. Figure 1b shows an optical micrograph of the main channel of the microfluidic chip filled with the dye and the square-shaped embedded deformable clamps which were not actuated. After actuation of a single square-shaped clamp with nitrogen gas (3 bar), the membrane of PDMS between the gas and fluid channel deflected toward the glass substrate deflecting the fluid flow regime in the actuated region (Figure 1(c)). Nonetheless, the dye stream could still flow through the clamp sides as shown in Figure 1c with black arrows. This noninterrupted flow condition

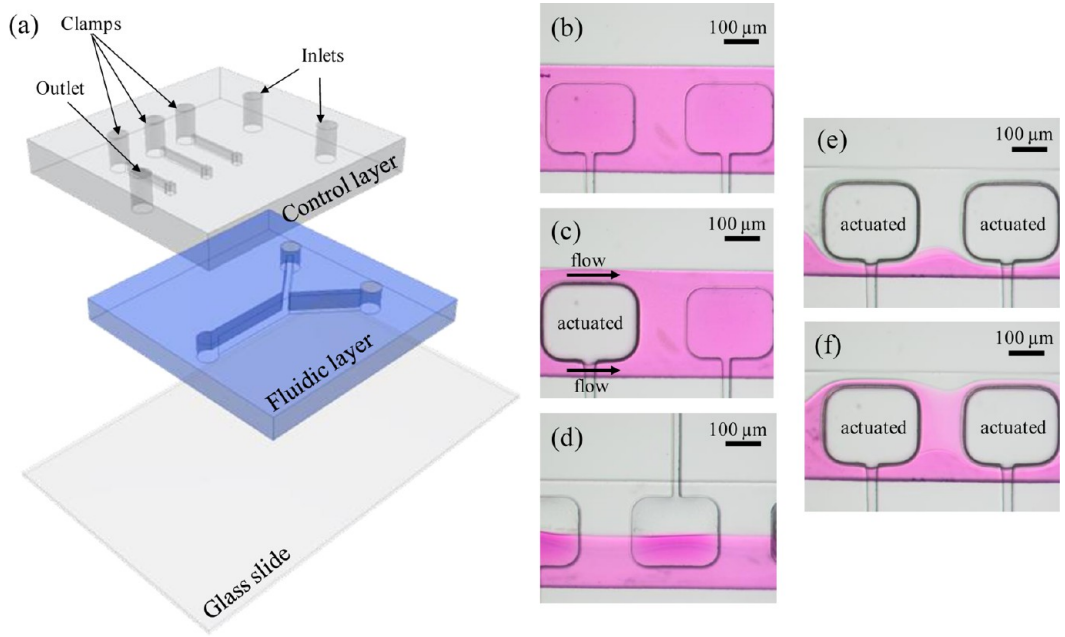

Figure 1. (a) Schematic view of the multilayer microfluidic chip used in our experiments. (b) Optical microscope image of the microfluidic chip filled with an aqueous solution of rhodamine dye. (c) An optical micrograph showing the actuation of the pneumatic clamp located on the left. The arrows indicate the fluid flow around the squared-shape valve design. (d) Optical microscope image of the laminar flow regime achieved by coflowing a water stream to the dye flow. (e and f) optical microscope images showing the tuning of the dye solution−water interface by varying one fluid flow rate when the valves are actuated. In panel e the dye flow rate is higher (30 μL/min) than the water flow rate (10 μL/min), whereas in panel f, the opposite is true.

is essential in order to allow an online, continuous, and sequential chemical event treatment of the trapped Ag(I)Cys CPs (*vide infra*). We further demonstrated the laminar flow regime with the injection of a second fluid stream; water (Figure 1d). When the clamps were actuated under a laminar flow regime, a precise guiding of the water and dye interface could be achieved by varying the relative flow rates. Figure 1e and Figure 1f show that when the flow rate of the dye solution stream is lower, a down-shifted guiding of the interface could be accomplished; whereas at higher dye flow rates the interface was shifted upward in the optical micrograph image. This accurate control of the interface position inside the microfluidic channel is very promising for a precise localization of the coordination pathway which leads to the formation of Ag(I)Cys CP (*vide infra*).

With this microengineered fluidic clamp-based chip in hand, we employed it both to localize *in situ* synthesis of the Ag(I)Cys CP and to induce a site-specific growth of functional Ag(I)TCNQ nanowire bundles on the underlying surface. In a typical experiment two aqueous reagent solutions, $Ag(NO_3)$ (2.5 mM) and Cys (2.5 mM), were injected through the fluidic channel at flow rates of 50 μL/min. The concentration of the reagent precursors was optimized to avoid channel clogging. Figure 2a shows a sequence of optical microscope images of the interface of the two coflowing reagent streams where the formation of Ag(I)Cys CP occurred (indicated with green arrows). Actuation of a microfluidic pneumatic clamp at 3 bar enabled both a localized trapping of Ag(I)Cys CP on the glass substrate surface (Figure 2b) and a successful removal of all surplus reagents solutions used during the synthesis of Ag(I)Cys CP, washed away with a flow of pure water (Figure 2i). Afterward, a saturated ascorbic acid solution in EtOH was added to the microfluidic platform (10 μL/min) in order to reduce the monovalent silver salt to the metal. To favor a precise chemical treatment of the trapped Ag(I)Cys CP underneath the clamped area, the clamp pressure was reduced to 1 bar (Figure 2ii). As shown in Figure 2b, a clear color change to a darker brown was demonstrated after treating the trapped Ag(I)Cys CP with the solution of ascorbic acid for approximately 2 min. The color change was attributed to the reduction of Ag(I) to metallic silver (Ag(0)) by the ascorbic acid, a supposition that was corroborated with bulk powder X-ray diffraction (PXRD) studies (Supporting Information, Figure S1), and in accord with previous observations.[26−29] It is worth noting that the color change assigned to the silver reduction was only observed underneath the clamp area, thereby demonstrating the localized chemical treatment enabled by the present approach (Figure 2c). After this reduction step, a washing procedure with ethanol was necessary in order to eliminate the excess ascorbic acid in the microfluidic channel (Figure 2iii). An increase of the clamp pressure to 3 bar was necessary during this rinsing process in order to avoid the movement and elution of the material. Washing steps between consecutive chemical reactions turned out to be crucial as they ensure that no additional

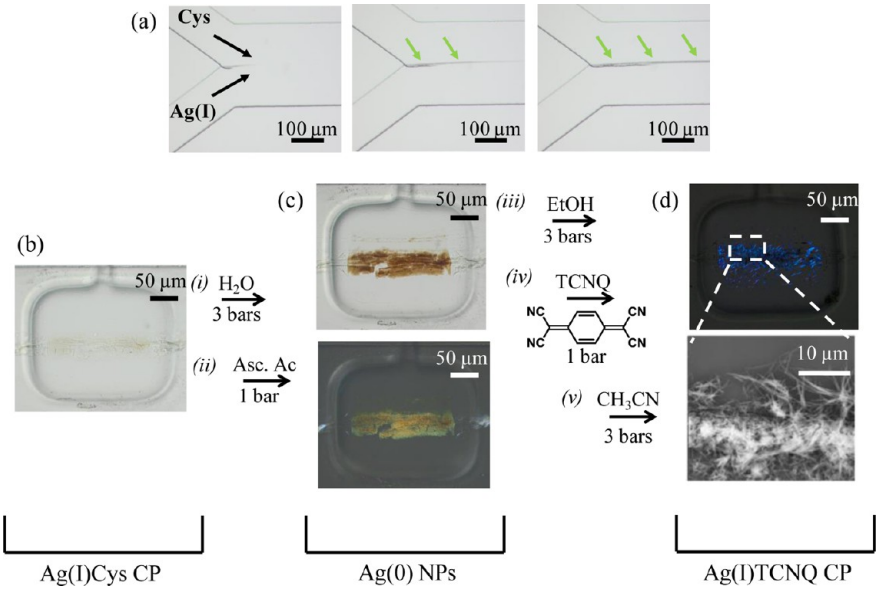

Figure 2. (a) A sequence of optical microscope images showing the assembly of Ag(I)Cys CP at the interface of $Ag(NO_3)$ and Cys aqueous reagent streams. The yellow arrows indicate the Ag(I)Cys CP assembled at the interface of the two coflowing streams. From panels b to d, optical microscope images showing the five consecutive chemical events (i, ii, iii, iv, and v) that lead ultimately to the self-supported growth of Ag(I)TCNQ nanowires. (b) An optical micrograph showing trapped Ag(I)Cys CP. (c) A nonpolarized microscope image (top) and a polarized microscope image (bottom) of reduced Ag(I)Cys CP. (d) Polarized microscope image of Ag(I)TCNQ nanowires bundles (top) together with a SEM image showing the nanometer scale Ag(I)TCNQ wires that are grown (bottom).

reactions with surplus reagents could occur. Next, an oxidation of the deposited Ag(0) with TCNQ in acetonitrile was conducted after the clamp pressure was again set to 1 bar. In fact, the Ag(0) deposit acts as nucleation sites for the Ag(I)TCNQ charge transfer complex growth. The confirmation of the formation of the crystalline Ag(I)-TCNQ CPs was immediately clear under inspection with a polarizing optical microscope where polarization-dependent crystal colors were observed. Figure 2d (top) shows an optical microscope image taken using crossed polarizers showing a deep blue-purple color which is attributed to the crystalline Ag(I)TCNQ CPs. Furthermore, PXRD analysis on the sample removed from the chip corroborated the formation of the Ag(I)TCNQ complex in its tetragonal phase, which has been reported (Supporting Information, Figure S1).[30] To demonstrate that the crystalline Ag(I)TCNQ CP was formed from reduced Ag(I)Cys CP, a control experiment was performed where the chemical treatment with saturated ascorbic acid solution was omitted. In this case, no Ag(I)-TCNQ CPs were observed even after a long treatment time with a TCNQ solution. These results clearly evidence that the reduction of silver metal ions is necessary for Ag(I)TCNQ charge transfer complex growth. To avoid formation of TCNQ crystals after solvent evaporation, pure acetonitrile was injected into the microfluidic platform to wash away the remaining TCNQ solution while the clamp pressure was switched to 3 bar again (Figure 2v). Because it is inherently difficult to distinguish nanoscale Ag(I)TCNQ CP structures under the optical microscope, scanning electron microscopy (SEM) studies on released nonbonded

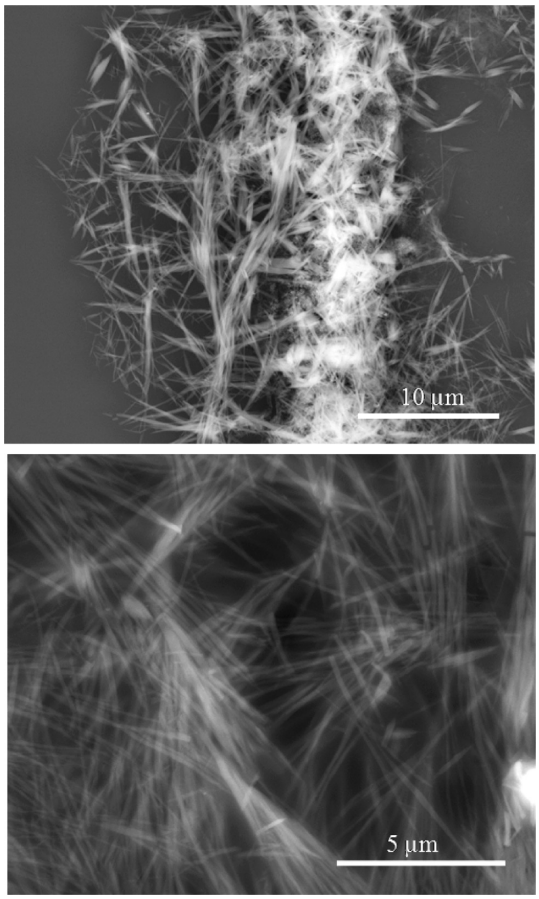

Figure 3. SEM images of Ag(I)TCNQ nanowire bundles synthesized with the presented clamp-based microfluidic approach.

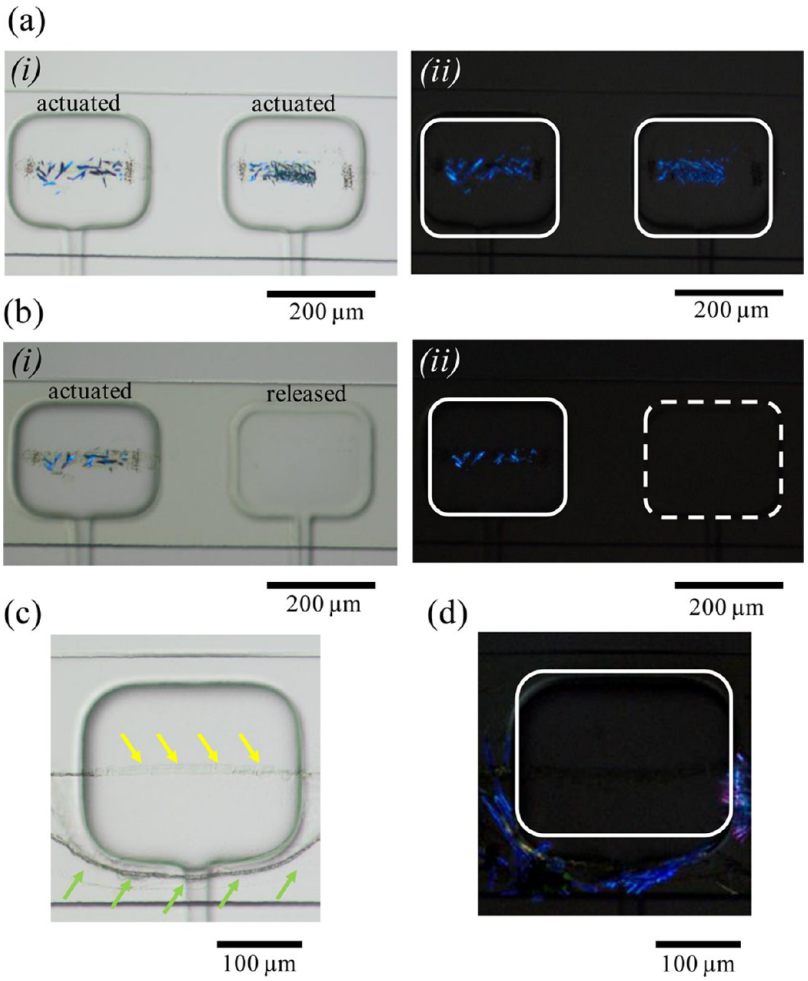

Figure 4. (a) Optical graphs showing a sequential templated growth of Ag(I)TCNQ nanowire bundles at different latitudes in the channel, (i) without, and (ii) with crossed polarizers. (b) (i) Micrograph showing the release of one valve, the second valve, and the wash away process of the Ag(I)TCNQ nanowire bundles located underneath. In panel ii, the same optical microscope image but with crossed polarizers. Notice that the squared-shape feature represented with a dash line represents the situation where the clamp is released, and with a solid line when it is actuated. (c) Optical microscope image of a double Ag(I)Cys CP guided assembly one synthesized before clamp actuation (yellow arrows), and the second after its actuation (green arrows). (d) Micrograph under crossed polarizers showing the templated growth of Ag(I)TCNQ nanowire bundles only on the Ag(I)Cys CP outside the clamp region.

chips were conducted. Clearly, SEM characterization demonstrated the nanoscale nature of the crystalline Ag(I)TCNQ CPs grown with this microfluidic-assisted template method where a localized ligand exchange is facilitated (Figure 2d, bottom image, and Figure 3). Typical diameters of these Ag(I)TCNQ nanowires range from 60 to 250 nm, and the length can be longer than 10 μm.

A parallelized Ag(I)TCNQ patterning on a glass surface was also demonstrated with this clamp-based approach. Figure 4a shows optical micrographs of the Ag(I)TCNQ CPs grown and located precisely underneath two clamp patches. Images with parallel and crossed polarizers are shown in Figure 4a,i and Figure 4a,ii, respectively. By releasing the second valve and additionally increasing the acetonitrile flow rate from 10 μL/min to 50 μL/min and above, a controlled removal of Ag(I)TCNQ from the glass surface was demonstrated (Figure 4b,i and 4b,ii). Interestingly, if the flow rates were interrupted, the two valves could be released and the Ag(I)TCNQ CPs remained in place and on the surface (Supporting Information, Figure S2). This result was very important not just to show the potential of the template growth approach toward surface patterning, but to further demonstrate the possibility of integrating the Ag(I)TCNQ nanowires onto electrode arrays located on the glass surface (vide infra).

Additionally, by controlling the clamp pressure and the interface position during the formation of the Ag(I)Cys CP, a precise templated growth of Ag(I)TCNQ could be achieved. Figure 4c shows an optical micrograph of Ag(I)Cys CP formed under laminar flow conditions, which was trapped by the clamp actuation (indicated with yellow arrows in the figure), and Ag(I)Cys CP formed outside the clamp region after this was actuated (denoted with green arrows). We demonstrated that when all five consecutive chemical events described in Figure 2, from i to v, were conducted with a clamp pressure of 3 bar, an accurate templated Ag(I)TCNQ

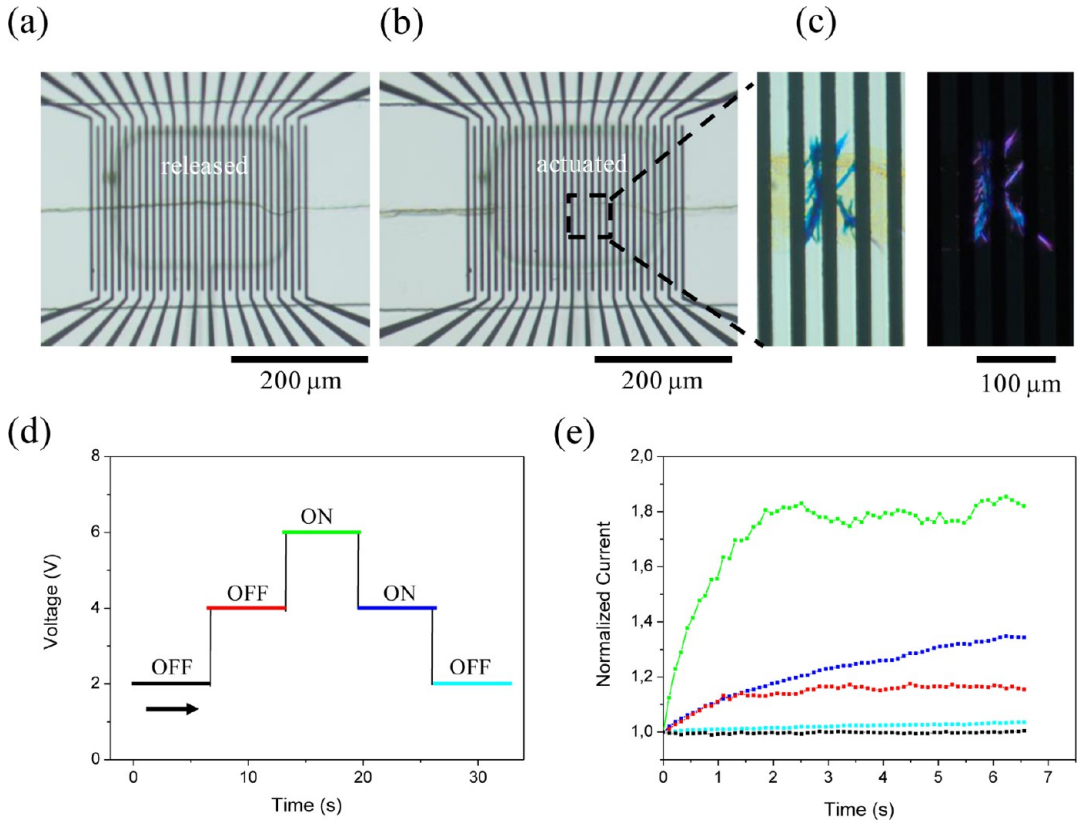

Figure 5. (a) Optical microscope image showing the synthesis of Ag(I)Cys CP over a patterned electrode surface, and in (b) a micrograph upon the pneumatic actuation. (c) Optical microscope images of Ag(I)TCNQ nanowire bundles under nonpolarized light (top) and under cross-polarized illumination (bottom). (d) Schematic illustration of the reversible voltage cycle applied to the Ag(I)TCNQ nanowires and in (e) the normalized current signal response measured.

growth was accomplished only on the Ag(I)Cys CP located outside the valve region (Figure 4d). This localized site-specific templated growth is extremely encouraging because it provides the best evidence of the control enabled by the present approach toward a precise crystal template growth process due to its excellent fluid control. Importantly, in the present case, the template growth process was performed at lower flow rates of both reactants and washing solvents (maximum 2 μL/min) in order to avoid the elution of Ag(I)Cys CP from the chip. Notice that even though the flow rates used during the five consecutive chemical events were low, the Ag(I)Cys CP located outside the clamp region moved slightly from its initial position (Figure 4b,ii). Besides thermal vapor deposition methods, the number of template techniques which facilitate rapid and consecutive chemical events to be addressed at specific locations and with excellent fluid handling conditions is very limited. To the best of our knowledge, there are no other methods described where an amino acid-supported framework is employed for the synthesis of functional crystalline matter with such a control in both the location of the scaffold enabling the template growth, and guiding the consecutive chemical events in a "one-pot" format.

Studies conducted with lower concentrations of $Ag(NO_3)$ (1.0 mM) and Cys (1.0 mM) precursor solutions corroborated the formation of a smaller number of Ag(I)TCNQ nanowires from the trapped Ag(I)Cys CP, probably due to the lower amount of Ag(I)Cys CP trapped under these conditions (Supporting Information, Figure S3). Interestingly, adjusting the concentration to 1.0 mM enabled a clear time-sequence analysis of the oxidation process (Supporting Information, Figure S4). In these investigations, it was demonstrated, under optical microscope visualization, that around 30 min were necessary to conclude crystalline Ag(I)TCNQ charge transfer complex growth. Moreover, these studies indicated that with this approach a continuous growth of Ag(I)TCNQ nanowire bundles up to 40 μm far away from its initial interface was possible. The small number of Ag(I)TCNQ nanowires at this concentration facilitated this study. Notably, no observation of Ag(I)TCNQ CPs was evidenced at a lower concentration of reagents (data not shown), hence delimiting the concentration range of the precursor solutions from which a clear appreciation of the growth process was feasible.

As stated above, pneumatic clamp actuation can also be employed for a selective localization and integration of Ag(I)TCNQ charge transfer complexes on patterned electrode surfaces. In these experiments, a glass surface containing an electrode array was used during the templated growth process. The electrode

array was perfectly aligned below the square-shape valves in order to favor Ag(I)TCNQ integration (Figure 5, and Supporting Information, Figure S5a). To confirm the integration of Ag(I)TCNQ nanowire bundles to the electrode array, microscale two-point electrical measurements (Figure 5 and Supporting Information, Figure S5b), and current sensing atomic force microscopy (CS AFM) studies were conducted on different samples (Supporting Information, Figure S5c). Figure 5 shows, from panels a to c, an Ag(I)TCNQ template growth process conducted on a patterned electrode glass surface. Figure 5d presents a schematic illustration of a reversible voltage cycle applied to the Ag(I)TCNQ nanowires, and Figure 5e shows a representative and normalized current signal response measured at different voltage steps, 2, 4, and 6 V. Figure 5e clearly supports the assertion that the Ag(I)TCNQ bundles grown with this methodology have indeed high (ON) and low (OFF) current states which can be accurately switched by controlling the voltage applied to the electrodes. A characteristic two-order-fold increase in current (ON state) was evidenced at 6 V,[31] therefore confirming the effective assembly of functional Ag(I)TCNQ memory elements with this microfluidic-assisted template method. In contrast, at 4 V the current change between the ON and OFF states was lower than at 6 V, indicating the reversible hysteretic switching behavior of the Ag(I)TCNQ material (see also Supporting Information, Figure S5b). Furthermore, CS AFM studies confirmed beyond doubt the integration of Ag(I)TCNQ nanowire bundles to the electrode array with the acquisition of current maps where nanowire features were clearly appreciated (Supporting Information, Figure S5c).

CONCLUSIONS

Both continuous chemical events and a controlled crystal template growth are possible with a clamp-based microfluidic approach. We have thus proven that microengineered pneumatic clamps can be exploited for functions which go far beyond a simple trapping of *in situ* formed structures. A unique and straightforward synthetic route for producing functional and crystalline Ag(I)TCNQ nanowire bundles from an amino acid-supported coordination framework (Ag(I)Cys CP) has been described, where mild conditions were used. The Ag(I)TCNQ nanowire bundles were generated online within a single microfluidic channel and on surface. Furthermore, a precise localization and integration of conductive Ag(I)TCNQ nanowire bundles to electrode arrays located underneath the clamp area was demonstrated. Thus, unlike other techniques where the material is formed upon evaporation,[32] where electrodes are evaporated onto existing nanostructures,[31] or where electrophoretic methods are used to align orientation but not position,[33] this soft bottom-up approach allows the parallel template formation of molecular nanostructures from solution on device surfaces with no need for postassembly manipulation to reach the functioning system.

It is important to note that the control of clamp pressure and in parallel the variation of relative flow rates of source solutions can in principle lead to spatially controlled deposition of materials at different locations on a chip. The *in situ* reaction and washing procedures make this approach a powerful one for the fabrication of multicomponent complex systems. We envision the use of the present method to a variety of other systems and structures, therefore expanding and opening up new powerful routes for a localized synthesis and integration of other functional hybrid systems which could further be employed in optoelectronic applications, sensing, and catalysis. Indeed, the results presented here should also open new possibilities in the ambitious route of biomolecular scaffolding and device fabrication.

MATERIALS AND METHODS

All reagents were purchased from Sigma-Aldrich Co. High purity solvents were purchased from Teknokroma, and used without further purification. Deionized Millipore Milli-Q water was used in all experiments.

Fabrication of patterned electrode surfaces on glass coverslips. The electrodes consisted of a chromium adhesion layer (Cr (10 nm)) and a top platinum layer (Pt) 100 nm thick. These electrodes were fabricated on substrates of glass coverslips with standard UV-photolithography and lift-off using acetate transparency as a mask (JD Photo-Tools, UK) and 1.7 μm thin AZ 5214 E photoresist (Clariant, GmbH).

Two-layer microfluidic chip assembly. The two polydimethylsiloxane (PDMS) layers were fabricated on silicon wafers (Okmetic, Finland) with SU8-2025 as photoresist (Microchemicals, GmbH) using conventional soft lithography techniques.[25] Both, the fluid and control layer had features 50 μm high as confirmed by profilometry measurements. The top (control) layer was fabricated by a replication molding technique,[34] where a PDMS oligomer and hardener mixture (5:1 in weight) was poured onto the "control layer" wafer bearing the SU-8 features and polymerized at 80 °C for 30 min. Next, the bottom (fluid channel) layer was spin-coated at 2000 rpm for 1 min with a PDMS oligomer and hardener mixture 20:1, respectively. After spinning the PDMS mixture, the "fluidic" master was cured at 80 °C over 10 min. Later, 1.0 mm holes were punched in the control layer with a biopsy punch (Miltex GmbH) and this was then assembled on top of the cured fluidic layer present in the "fluidic" master. The two layers were then placed in an oven at 80 °C overnight in order to enable the bonding process. After that, the two bonded layers were removed from the "fluidic" master and 1.5 mm holes were punch in the fluidic layer. A final assembly of the two bonded layers to a glass coverslip (24 mm × 60 mm) was finally achieved through oxygen plasma activation of the two parts.

Instrumentation. Pt−Cr electrodes and fluidic masters were obtained by standard photolithography by using a DELTA 80 spinner (Süss), a Karl Suss MA/BA6 mask aligner, and an electron-assisted metal evaporator UNIVEX 450B (Oerlikon Leybold Vacuum). X-ray powder diffraction (XRPD) measurements were performed with an X'Pert PRO MPD diffractometer (Panalytical).

SEM measurements. All SEM images presented in this work were acquired on a SEM QUANTA FEI 200 FEG-ESEM operating in a low vacuum mode. In all cases the samples were measured as prepared with no need of metal deposition on the samples.

Electrical characterization and CS AFM studies. Two-point electrical characterizations were performed using a two channel Keithley 2612 SourceMeter and were measured under ambient conditions. On the other hand, CS AFM studies were performed on a 5500LS SPM system from Agilent Technologies using the Resiscope module. Unlike the two-point electrical characterization, a nanoscaled conducting tip was biased to the electrode array patterned on the glass coverslip. In this case, the current flowing through the electrodes to the integrated Ag(I)TCNQ nanowire bundles was measured with a conductive grounded tip at each point of the image, thus providing a current map image of the region scanned.

Conflict of Interest: The authors declare no competing financial interest.

Supporting Information Available: Additional optical micrographs, X-ray diffractograms of the materials, as well as electrical characterization of Ag(I)TCNQ prepared here. This material is available free of charge *via* the Internet at http://pubs.acs.org.

Acknowledgment. This research was supported by the MINECO, Spain (Projects CTQ2010-16339, MAT2012-30994, and CTQ2011-16009-E)), and the DGR, Catalonia (Project 2009 SGR 158). J.P.L. and I.I. thank the MINECO for a Ramón y Cajal Contract (RYC-2011-08071 and RYC-2010-06530, respectively). J.P.L. also thanks funding from the European Community's Seventh Framework Programme under Grant Agreement No. PCIG-11-GA-2012-32139, (project MuLoPla). Ll. Abad gratefully acknowledges a JAE-Doc contract from CSIC partially funded by European Social Fund (ESF). The authors also thank Dr. Francisco Javier del Campo for useful discussions and the GICSERV-B Program: 8th call, IMB-CNM-CSIC, Spain (Project NGG-261).

REFERENCES AND NOTES

1. Briseno, A. L.; Mannsfeld, S. C. B.; Ling, M. M.; Liu, Sh.; Tseng, R. J.; Reese, C.; Roberts, M. E.; Yang, Y.; Wudl, F.; Bao, Z. Patterning Organic Single-Crystal Transistor Arrays. *Nature* **2006**, *444*, 913–917.
2. Xia, Y.; Yang, P.; Sun, Y.; Wu, Y.; Mayers, B.; Gates, B.; Yin, Y.; Kim, F.; Yan, H. One-Dimensional Nanostructures: Synthesis, Characterization, and Applications. *Adv. Mater.* **2003**, *15*, 353–389.
3. Wang, X.; Summers, C. J.; Wang, Z. L. Large-Scale Hexagonal-Patterned Growth of Aligned ZnO Nanorods for Nano-Optoelectronics and Nanosensor Arrays. *Nano Lett.* **2004**, *4*, 423–426.
4. Reches, M.; Gazit, E. Casting Metal Nanowires within Discrete Self-Assembled Peptide Nanotubes. *Science* **2003**, *300*, 625–627.
5. Zhang, L.; Li, N.; Gao, F.; Hou, L.; Xu, Z. Insulin Amyloid Fibrils: An Excellent Platform for Controlled Synthesis of Ultrathin Superlong Platinum Nanowires with High Electrocatalytic Activity. *J. Am. Chem. Soc.* **2012**, *134*, 11326–11329.
6. Huang, Z.; Pu, F.; Hu, D.; Wang, C.; Ren, J.; Qu, X. Site-Specific DNA-Programmed Growth of Fluorescent and Functional Silver Nanoclusters. *Chem.—Eur. J.* **2011**, *17*, 3774–3780.
7. Zhao, X.; Pan, F.; Xu, H.; Yaseen, M.; Shan, H.; Hauser, C. A. E.; Zhang, S.; Lu, J. R. Molecular Self-Assembly and Applications of Designer Peptide Amphiphiles. *Chem. Soc. Rev.* **2010**, *39*, 3480–3498.
8. Woolfson, D. N.; Mahmoud, Z. N. More Than Just Bare Scaffolds: Towards Multi-Component and Decorated Fibrous Biomaterials. *Chem. Soc. Rev.* **2010**, *39*, 3464–3479.
9. Pu, F.; Liu, X.; Xu, B.; Ren, J.; Qu, X. Miniaturization of Metal–Biomolecule Frameworks Based on Stereoselective Self-Assembly and Potential Application in Water Treatment and as Antibacterial Agents. *Chem.—Eur. J.* **2012**, *18*, 4322–4328.
10. Rubio-Martínez, M.; Puigmartí-Luis, J.; Imaz, I.; Dittrich, P. S.; Maspoch, D. "Dual-Template" Synthesis of One-Dimensional Conductive Nanoparticle Superstructures from Coordination Metal–Peptide Polymer Crystals. *Small* **2013**, 10.1002/smll.201301338.
11. Kitagawa, S.; Kitaura, R.; Noro, S.-i. Functional Porous Coordination Polymers. *Angew. Chem., Int. Ed.* **2004**, *43*, 2334–2375.
12. Yaghi, O. M.; O'Keeffe, M.; Ockwig, N. W.; Chae, H. K.; Eddaoudi, M.; Kim, J. Reticular Synthesis and the Design of New Materials. *Nature* **2003**, *423*, 705–714.
13. Narayan, T. C.; Miyakai, T.; Seki, Sh.; Dincă, M. Tetrathiafulvalene-Based Microporous Metal–Organic Framework. *J. Am. Chem. Soc.* **2012**, *134*, 12932–12935.
14. Deng, H.; Grunder, S.; Cordova, K. E.; Valente, C.; Furukawa, H.; Hmadeh, M.; Gándara, F.; Whalley, A. C.; Liu, Z.; Asahina, S.; et al. Large-Pore Apertures in a Series of Metal–Organic Frameworks. *Science* **2012**, *336*, 1018–1023.
15. Ameloot, R.; Roeffaers, M. B. J.; De Cremer, G.; Vermoortele, F.; Hofkens, J.; Sels, B. F.; De Vos, D. E. Metal–Organic Framework Single Crystals as Photoactive Matrices for the Generation of Metallic Microstructures. *Adv. Mater.* **2011**, *23*, 1788–1791.
16. Wang, Z.; Cohen, S. M. Postsynthetic Covalent Modification of a Neutral Metal–Organic Framework. *J. Am. Chem. Soc.* **2007**, *129*, 12368–12369.
17. Wang, Z.; Cohen, S. M. Tandem Modification of Metal–Organic Frameworks by a Postsynthetic Approach. *Angew. Chem., Int. Ed.* **2008**, *47*, 4699–4702.
18. Tanabe, K. K.; Wang, Z.; Cohen, S. M. Systematic Functionalization of a Metal–Organic Framework *via* a Postsynthetic Modification Approach. *J. Am. Chem. Soc.* **2008**, *130*, 8508–8517.
19. Nguyen, J. G.; Cohen, S. M. Moisture-Resistant and Superhydrophobic Metal–Organic Frameworks Obtained *via* Postsynthetic Modification. *J. Am. Chem. Soc.* **2010**, *132*, 4560–4561.
20. Puigmarti-Luis, J.; Rubio-Martinez, M.; Hartfelder, U.; Imaz, I.; Maspoch, D.; Dittrich, P. S. Coordination Polymer Nanowires Generated by Microfluidic Synthesis. *J. Am. Chem. Soc.* **2011**, *133*, 4216–4219.
21. Furukawa, S.; Hirai, K.; Nakagawa, K.; Takashima, Y.; Matsuda, R.; Tsuruoka, T.; Kondo, M.; Haruki, R.; Tanaka, D.; Sakamoto, H.; *et al.* Heterogeneously Hybridized Porous Coordination Polymer Crystals: Fabrication of Heterometallic Core-Shell Single Crystals with an In-Plane Rotational Epitaxial Relationship. *Angew. Chem., Int. Ed.* **2009**, *48*, 1766–1770.
22. Hirai, K.; Furukawa, S.; Kondo, M.; Uehara, H.; Sakata, O.; Kitagawa, S. Sequential Functionalization of Porous Coordination Polymer Crystals. *Angew. Chem., Int. Ed.* **2011**, *50*, 8057–8061.
23. Falcaro, P.; Hill, A. J.; Nairn, K. M.; Jasieniak, J.; Mardel, J. I.; Bastow, T. J.; Mayo, S. C.; Gimona, D.; Gomez, H. J.; Whitfield, R.; *et al.* A New Method to Position and Functionalize Metal–Organic Framework Crystals. *Nat. Commun.* **2011**, *2*, 237 (8 pages).
24. Chen, X.; Zheng, G.; Cutler, J. I.; Jang, J.-W.; Mirkin, C. A. In-Wire Conversion of a Metal Nanorod Segment into an Organic Semiconductor. *Small* **2009**, *5*, 1527–1530.
25. Cvetković, B. Z.; Puigmartí-Luis, J.; Schaffhauser, D.; Ryll, T.; Schmid, S.; Dittrich, P. S. Confined Synthesis and Integration of Functional Materials in Sub-nanoliter Volumes. *ACS Nano* **2013**, *7*, 183–190.
26. Velikov, K. P.; Zegers, G. E.; van Blaaderen, A. Synthesis and Characterization of Large Colloidal Silver Particles. *Langmuir* **2003**, *19*, 1384–1389.
27. Sondi, I.; Goia, D. V.; Matijević, E. Preparation of Highly Concentrated Stable Dispersions of Uniform Silver Nanoparticles. *J. Colloid Interface Sci.* **2003**, *260*, 75–81.
28. Rodríguez-González, B.; Burrows, A.; Watanabe, M.; Kiely, C. J.; Liz Marzán, L. M. Multishell Bimetallic AuAg Nanoparticles: Synthesis, Structure and Optical Properties. *J. Mater. Chem.* **2005**, *15*, 1755–1759.
29. Ma, Y.; Li, W.; Cho, E. C.; Li, Z.; Yu, T.; Zeng, J.; Xie, Z.; Xia, Y. Au@Ag Core–Shell Nanocubes with Finely Tuned and

Well-Controlled Sizes, Shell Thicknesses, and Optical Properties. *ACS Nano* **2010**, *4*, 6725–6734.
30. O'Kane, A.; Clerac, R.; Zhao, H. H.; Ouyang, X.; Galan-Mascaros, J. R.; Heintz, R.; Dunbar, K. R. New Crystalline Polymers of Ag(TCNQ) and Ag(TCNQF4): Structures and Magnetic Properties. *J. Solid State Chem.* **2000**, *152*, 159–173.
31. Ren, L.; Fu, L.; Liu, Y.; Chen, S.; Liu, Z. Electrochemical Synthesis of High-Quality Ag(I)TCNQ Nanowires Using Carbon Nanotube Electrodes. *Adv. Mater.* **2009**, *21*, 4742–4746.
32. Xiao, K.; Tao, J.; Puretzky, A. A.; Ivanov, I. N.; Retterer, S. T.; Pennycook, S. J.; Geohegan, D. B. Selective Patterned Growth of Single-Crystal Ag−TCNQ Nanowires for Devices by Vapor−Solid Chemical Reaction. *Adv. Funct. Mater.* **2008**, *18*, 3043–3048.
33. Xiao, J.; Yin, Z.; Wu, Y.; Guo, J.; Cheng, Y.; Li, H.; Huang, Y.; Zhang, Q.; Ma, J.; Boey, F.; *et al*. Chemical Reaction between Ag Nanoparticles and TCNQ Microparticles in Aqueous Solution. *Small* **2011**, *7*, 1242–1246.
34. Xia, Y.; Whitesides, G. M. Soft Lithography. *Annu. Rev. Mater. Sci.* **1998**, *28*, 153–184.